J. Phys. C 17, 5975 (1984).

Soliton Dynamics on an Easy Plane Ferromagnetic Chain

G. Wysin[†] and A.R. Bishop

Theoretical Division and Center for Nonlinear Studies*

Los Alamos National Laboratory

Los Alamos, NM 87545, USA

and

P. Kumar[††]

Department of Physics

University of Florida

Gainesville, FL 32611, USA

ABSTRACT

It is now generally accepted that the description of solitons in an easy plane ferromagnetic chain in terms of a sine Gordon theory is inadequate. The structural and dynamic properties of these solitons are not very clear. We present here results of a numerical simulation of the dynamics of a single soliton as well as collisions between a soliton-antisoliton pair. The dynamics of a single soliton appears to be consistent with variational method calculations. The energy dispersion (E(u) where u is the propagation velocity), consists of three continuously connected branches. Only the first branch is sine Gordon-like with an effective soliton mass. A soliton-antisoliton pair collision leads to a variety of final states. As a function

[†]Permanent address: LASSP, Clark Hall, Cornell University, Ithaca, NY 14853, USA.

*Work performed under the auspices of U.S. Department of Energy.

[††]Work supported by U.S. National Science Foundation under grant DMR-8006311.

of magnetic field (B), there are four major regimes. At very low fields, the pair transmit through each other similar to a pair collision for true sine Gordon solitons. For somewhat higher fields, the pair forms a bound state (breather mode) on collision. Further increase in magnetic field leads to reflection of the soliton-antisoliton pair. As a function of increasing collision velocity u_{sG} for an initial sine Gordon pair, the various critical fields decrease. Furthermore, there are details in the final state diagram (in the u_{sG}-B plane) that correspond to resonance scattering (for breather modes) and branch transfer (in the pair collison leading to reflection). Implications of these results for quasi-one-dimensional ferromagnets such as $CsNiF_3$ and

CHAB ($(C_6H_{11}NH_3)CuBr_3$) are suggested. In particular, we suggest that nonlinear elementary excitations in these chains are breathers rather than isolated solitons.

1. Introduction

Solitons in an easy plane ferromagnetic (EPF) chain have been a subject of considerable interest for several years (see various reviews by Steiner 1981, 1982). On the theoretical side, this interest came first from the possibility that the nonlinear excitations in an EPF could be described in terms of a sine Gordon (sG) theory (Mikeska 1978). Later it was predicted that the sG description had an instability (Kumar 1982; Magyari and Thomas 1982) and that the soliton properties were in fact more complex; a fact which added to the theoretical interest. On the experimental side, outside of superfluid ^{3}He, $CsNiF_3$ (a prototype EPF) was the first system (along with related anti-ferromagnetic chains) for which there was a demonstration of soliton effects. A considerable body of experimental literature now exists that includes observation of soliton effects in neutron scattering, specific heat and nuclear spin relaxation. Again the experimental activity also seems to be growing on account of the instability mentioned earlier.

From a theoretical point of view, the principal unknowns concern the properties of distorted solitons (i.e. solitons for which a sG description is inappropriate). We note briefly, the known properties of the distorted soliton. In the presence of an applied field perpendicular to the chain direction (and in the easy plane), the nonlinear excitations are the screw-like rotations of the spin. At low fields, the spins remain close to the easy plane as they rotate and these are the sG solitons. The instability refers to the propensity for spins to deviate strongly from the easy plane, thereby gaining exchange and Zeeman energies at the cost of the anisotropy energy. For a static soliton the instability occurs at $B = B_c = 2A/3$, where B is the magnetic field and A is the anisotropy energy (see section 2). However, the critical field rapidly decreases for a moving soliton and is only a small

fraction of B_c for a soliton moving with a velocity which is a fraction of the spin wave velocity (the maximum velocity). Thermodynamic quantities, such as the specific heat, have been calculated (Kumar and Samalam 1982) using the transfer matrix methods. While these provide an experimentally measurable quantity, they shed no light on the structure or dynamics of the distorted solitons. The motivation of this study is to elucidate those features.

The results reported here are from numerical simulations of a discrete EPF chain with two initial conditions: (a) a single sG soliton(S), launched with a given velocity (energy); and (b) a soliton-antisoliton ($S\bar{S}$) pair, approaching each other with an asymptotic velocity appropriate to their relaxed (distorted) profiles. In the absence of analytical methods, numerical simulation has been the traditional route to the understanding of strongly nonlinear phenomena. In the present case we are able to test the validity of various analytical Ansätze, which can form the basis for an understanding of the rather complex soliton structures and dynamics.

We find the single soliton excitations to be "multibranched"*. (See Fig. 1 and Section 2.) Given a magnetic field $B < B_c$ and a propagation velocity, there are two possible soliton solutions with different energies. Only the lower branch can be sensibly understood in terms of perturbed sG solitons. For $B > B_c$, the lower energy solution ceases to exist. The higher energy solutions are far from sG-like. The results for $S\bar{S}$ collisions are equally striking. Whereas at low fields and intermediate collision velocities, the collisions are sG-like (the solitons pass through each other), at moderate fields they form breather like bound states. At even higher

*Note that the kink dispersion appears to be perfectly continuous. The separation into "branches" is therefore for descriptive convenience only.

fields, the collision results in the reflection of solitons which move on a third "branch" to be described in detail in section 3. Preliminary results from a single soliton simulation have been reported earlier (Wysin et. al, 1982). Here we describe some corrections to those results which are possible becase of improved numerical procedures (section 3).

The material in this paper is divided into two parts. In section 2, we describe the known analytical properties. These include a description of the Hamiltonian, the equations of spin dynamics and properties of a single soliton (based on a variational Ansatz) over essentially the entire field range. In section 3, we describe the results from our numerical simulation. These include results for a single soliton dynamics, largely in agreement with analytical results, and the pair collision. Finally, section 4 consists of a summary of our conclusions and a brief discussion of their implications for experiments and future analysis.

2. Model

The system we consider is described by the Hamiltonian

$$H = -J \sum_n \vec{S}_n \cdot \vec{S}_{n+1} + A \sum_n (\vec{S}_n^z)^2 - g\mu_B \vec{B} \cdot \sum_n \vec{S}_n, \qquad (1)$$

where $\vec{S}_n$ are dimensionless spin vectors at lattice sites n. The first term denotes the exchange energy with exchange constant $J > 0$, the second term represents the easy-plane (x-y) anisotropy energy with $A > 0$, and the last term describes the effect of an external magnetic field (hereafter chosen to be in the x-direction). g and μ_B are the Landé g factor and the Bohr magneton respectively. The dynamics of these spins is described by the undamped Bloch equation

$$\hbar \dot{\vec{S}}_n = \vec{S}_n \times \vec{F}_n \qquad (2.a)$$

where

$$\vec{F}_n = J(\vec{S}_{n-1} + \vec{S}_{n+1}) + g\mu_B \vec{B} - 2AS_n^z \hat{z} \qquad (2.b)$$

and $\hat{z}$ is a unit vector in the z-direction. $\vec{S}_n \times \vec{F}_n$ represents the torque on the spin at site n. In terms of the polar coordinates of the spin vectors $\vec{S}_n$ (i.e. θ, ϕ are out-of-plane and in-plane angles, respectively), the equations of motion become

$$\frac{\hbar}{JS} \dot{\phi}_n \cos\theta_n = \sin\theta_n \{\cos\theta_{n+1} \cos(\phi_{n+1} - \phi_n) + \cos\theta_{n-1} \cos(\phi_{n-1} - \phi_n)\}$$

$$- \cos\theta_n(\sin\theta_{n+1} + \sin\theta_{n-1}) + \frac{2A}{J} \cos\theta_n \sin\theta_n + \frac{g\mu B}{JS} \sin\theta_n \cos\phi_n \qquad (3.a)$$

$$\frac{\hbar}{JS}\dot{\theta}_n = \cos\theta_{n+1}\sin(\varphi_{n+1}-\varphi_n) + \cos\theta_{n-1}\sin(\varphi_{n-1}-\varphi_n) - \frac{g\mu B}{JS}\sin\varphi_n \qquad (3.b)$$

where $\vec{S}_n = S\,[\cos\theta_n\cos\varphi_n, \cos\theta_n\sin\varphi_n, \sin\theta_n]$. These equations are for a discrete lattice. We have integrated them numerically for a variety of initial conditions. For each initial condition, the time evolution is determined by only two constants: $\alpha \equiv 2A/J$ and $\beta \equiv g\mu_B B/JS$.

In the continuum limit (where the length scale ratio $J/B \gg 1$), Eqs. (3.a) and (3.b) can be reduced to the partial differential equations

$$\phi_\tau\cos\theta = -\theta_{\xi\xi} + (1-\phi_\xi^2)\sin\theta\cos\theta + b\sin\theta\cos\phi \qquad (4.a)$$

$$\theta_\tau = \phi_{\xi\xi}\cos\theta - 2\theta_\xi\phi_\xi\sin\theta - b\sin\phi, \qquad (4.b)$$

where $\xi^2 = \frac{2A}{Ja^2}z^2$ and $\tau = \frac{2AS}{\hbar}t$.

Here a is the lattice spacing and subscripts denote differentiation. In the continuum limit only <u>one</u> constant, $b=\beta/\alpha = \frac{g\mu_B B}{2AS}$, is needed to specify the time evolution (as opposed to the discrete lattice case above). In the limit $\theta, b \ll 1$, Eqs. (4) can readily be seen to reduce to the sG equation:

$$\phi_{\xi\xi} - \phi_{\tau\tau} = b\sin\phi \qquad (5.a)$$

$$\theta = \phi_\tau, \qquad (5.b)$$

whose solutions are the well known sG solitons, breathers and small amplitude oscillations (spin waves).

To go beyond the sG limit, we note that Eqs. (4) can be obtained from a

Lagrangian:

$$L = \varepsilon_o \int d\xi \left\{ \frac{1}{2} \left(\theta_\xi^2 + \varphi_\xi^2 \cos^2\theta \right) + \frac{1}{2}\sin^2\theta - b\cos\theta\cos\varphi - \varphi_\tau \sin\theta \right\}$$

where

$$\varepsilon_o = \sqrt{2AJ}\, S^2 \quad . \tag{6}$$

(Strictly speaking L is the negative of a Lagrangian and thus its minimum determines the trajectories). An expansion of Eq. (6) in terms of the fluctuations about a sG soliton is the basis of a stability analysis described elsewhere (Kumar 1982b, Magyari and Thomas 1982). It results in a static soliton instability field b_c=1/3 and $b_c(0)-b_c(u) \approx u^{2/3}$, where u is the soliton velocity. We can also calculate the soliton effective mass, m*, for $b \ll b_c$: for small u, the stability analysis yields the energy E(u) of the moving soliton as

$$E(u) = E(o) + \frac{1}{2} m^* u^2 \tag{7}$$

with

$$\frac{m^*}{m} = \frac{b_c}{b_c - b}. \tag{8}$$

It is possible to obtain variational solutions which relax the assumption of small deviation from a sG profile. Several Ansätze have been introduced in the literature. The most recent and appealing effort along these lines is due to Liebmann et. al.(1983). In a variational calculation, the choice of the trial function is all important. Liebmann et. al.'s choice of a trial spin profile for a soliton appears to avoid many of the difficulties associated

with previous approaches. More specifically, their Ansatz is (S_x, S_y, S_z are the spin cartesian components):

$$\begin{aligned} S_x(X) &= 1-c^2\left(1-\cos\Phi(X)\right) \\ S_y(X) &= c\sin\Phi(X) \\ S_z(X) &= cs\left(1-\cos\Phi(X)\right) \end{aligned} \tag{9}$$

where $\sin\Phi/2 = \mathrm{sech}X;\ X=(\xi-u\tau)/w.$

Here $c=\cos\Theta_m/2$, $s=\sin\Theta_m/2$ and Θ_m and w are the variational parameters. Θ_m represents the maximum excursion out of the easy plane at the soliton center. The angles Θ_m and Φ here differ from the notation used elsewhere in this paper. In particular, note that Θ_m is a number, not a z-dependent function.

The soliton dispersion following from Eq.(9) can be divided for convenience into three different branches (see Fig. 1): (i) for $b<b_c$ and $E(u)-E_{sG}(o)<<E_{sG}(o)$, the soliton motion is sG-like with the effective mass in Eq. (8). This branch, which we refer to as branch I, terminates at a maximum velocity $u=u_m(b)$; (ii) The soliton propagation for $E>E(u_m)$ corresponds to branch II where u decreases with increasing E, leading finally to a second static soliton with an energy higher than $E_{sG}(o)$ and with $\Theta_m=\Theta_o$ such that $E(\Theta_o)$ is the maximum energy for a soliton. The field dependence of the energy of the static soliton and the excursion angle Θ_o are given by

$$\begin{aligned} E &= E_{sG}(o)\ (2/3 + b)\left[1/3 + 2/(9b)\right]^{1/2} \\ \sin^2\Theta_o/2 &= (1/3-b); \end{aligned} \tag{10}$$

(iii) Finally, on branch III the solitons are moving with a negative velocity (relative to sG). It can be shown that the energy dispersion (E(u)) in the vicinity of the higher energy static soliton must necessarily be an inverted parabola: The effective mass in this region can be written in general as

$$m^{**} = \left. \frac{\frac{\partial}{\partial \Theta_m}(L-E)}{\frac{\partial^2 E}{\partial \Theta_m^2}} \right|_{\Theta_o} \tag{11}$$

and, since $E(\Theta_o)$ is a maximum, m^{**} must be negative. For $b>b_c$, only branch III survives; the soliton energy is always less than the sG rest mass $E_{sG}(o)$ (see Fig. 1). The Liebmann, et. al. Ansatz for the effective mass of this soliton yields

$$m^{**} = -\pi\sqrt{b/3}\,\left(\tfrac{1}{3}-b\right)^{-1} \quad , \quad b<b_c \tag{12.a}$$

$$= \frac{\pi}{2b}\left(\tfrac{1}{3}-b\right)^{-1} \quad , \quad b>b_c \quad . \tag{12.b}$$

To summarize, Eq. (12.b) yields the effective mass for a soliton at the energy extremum about $\theta_m = 0$. This is the branch I soliton for $b<b_c$ and branch III for $b>b_c$. Eq. (12.a) refers to the energy maximum solution about $\theta_m = \theta_o$ and it corresponds to a branch III soliton for all b ($< b_c$) since $\theta_o \to o$ as $b \to b_c$.

3. Numerical Simulations

The discrete equations of motion (Eqs. (3)) were integrated numerically on a lattice ranging between 100 and 180 spins. (The numbers of spins had to be increased at low magnetic fields in order to accomodate the wider solitons.) Periodic boundary conditions were used in all cases. Energy conservation was used as a test of the computational accuracy (better than 1 part in 10^5). The sG single soliton and soliton-antisoliton pairs were used as initial conditions. Since these initial conditions do not correspond to an exact solution of Eqs. (3), the short time results showed relaxation, involving emission of spin waves (particularly on branches II and III). In order to approach the isolated single soliton more accurately before making any measurements, we removed the energy contributions of the spin waves by time-averaging in the soliton's reference frame for a sufficiently long time. This scheme is very successful in all but the most extreme circumstances where the maximum out-of-plane angle approaches $\pi/2$ and the soliton width approaches a single lattice spacing. The results shown in Figs. (1)-(3) are an important improvement on the estimates contained in our earlier report (Wysin et. al. 1982), and in good agreement with the Ansatz of Liebmann et. al. (1983). (This agreement is less surprising since our averaging scheme produces accurate traveling-wave kink forms.) In order to test the validity of various continuum theories, most calculations were performed with $\alpha=2A/J=.0954$. Exceptions are indicated explicitly in the figures. This choice of α minimized the various discrete lattice effects. We comment later on the behaviour expected for an exchange constant appropriate to $CsNiF_3$ or CHAB.

a. Single Soliton Dynamics

Some of the results of this section have been reported earlier (Wysin et. al., 1982). We summarize them below for completeness, because they have direct bearing on the soliton-antisoliton collisions, and because of new refinements in our numerical procedures (above). The motion of solitons was observed starting from an initial sG soliton:

$$\tan\phi/4 = \exp\left[\gamma\sqrt{b}(\xi - u_{sG}\tau)\right], \tag{13}$$

where $\gamma = \left[1-u_{sG}^2\right]^{-1/2}$, and $\Theta = \phi_\tau$

and following the time evolution via Eqs. (3). The discrete lattice time evolution requires specification of α and β. A series of runs was performed holding α fixed (above) but varying β and u_{sG}, the velocity of the input sG soliton (and therefore energy). The soliton velocity was measured by identifying the center of the soliton as the point at which $\phi=\pi$. The oscillations in the soliton velocity were averaged numerically and this average velocity was identified as the soliton's propagation velocity. The average velocity u always satisfied $u<u_{sG}$ even for arbitrarily low u_{sG} and $b<<b_c$.

It was found that the soliton motion for $b<b_c$ could be classified into three different regions ("branches") according to the size of the out-of-plane angle, as explained in section 1. For very low energy, the soliton behaved rather similarly to the sG soliton. Its energy dispersion was accurately given by Eq. (7) with the effective mass given by Eq. (8). This branch (branch I) exists only for small u, more precisely for $u<u_m(b)$. The relationship between the maximum velocity u_m and b agrees with the

calculations of Magyari and Thomas (1982) and Kumar (1982b). For $E(u)>E(u_m)$, the progapating solitons belong to another branch (branch II). On this branch, the energy of the soliton increases with decreasing velocity. The further continuation of this branch (to branch III) leads to backward moving solitons with monotonicaly decreasing energy. All of these results are consistent with the predictions of Liebmann et. al. (1983). Figs. (2) and (3) show the field dependence of the maximum angle of excursion, θ_m, and the energy E of the higher energy static soliton respectively. The solid lines are based on the Liebman et. al. Ansatz, as given in Eq. (9). Note that this Ansatz slightly overestimates the energy as we should expect.

b. Soliton-Antisoliton Collision

The soliton-antisoliton ($S\bar{S}$) pair collision can be initiated by starting with a sG $S\bar{S}$ pair that is allowed to evolve in time according to the equations of motion (3) with α and β specified. The initial data then corresponds to

$$\phi(\xi,\tau) = 4 \tan^{-1} \left\{ \frac{\sinh\left(\gamma\sqrt{b}\, u_{sG}(\tau-\tau_o)\right)}{u_{sG} \cosh\left(\gamma\sqrt{b}\, \xi\right)} \right\}$$
$$\theta(\xi,\tau) = \phi_\tau. \qquad (14)$$

The value of the parameter τ_o determines the initial separation of the pair. If the pair were to move precisely according to sG dynamics, τ_o would represent the time before a collision. Since a soliton moves more slowly ($u<u_{sG}$), the actual time of collision is later. The final states (after the collision) were observed for times roughly 10 times the initial collision time. We show in Fig. (4) the variety of final states observed in the form of a phase diagram in the u_{sG}-b plane. The initial velocity u_{sG} can be interpreted as the input energy. This phase diagram consists of four major

regions:

(1) Region I: For low fields, $b<b_1(u_{sG})$, the $S\bar{S}$ pair collision is essentially sG like (e.g. Fig. 5a). The solitons pass through each other with little distortion of profile and therefore essentially no asymptotic change in velocity. This is consistent with the low b expectations for single solitons (Fig. 1). However, the largest b field where sG like transmission takes place is only $b_{1(max)} \simeq 0.06$ (corresponding to $u_{sG} = 0.5$ and u (actual) $\simeq 0.3$). An interesting effect appears for small u_{sG}, in that $b_1 (u_{sG} \to 0) \to 0$. In other words, while one might expect the sG characteristics to remain intact at low velocities, they do not. Instead, the low velocity collision even at low fields leads to the formation of a breather. This is presumably a balance of collision time versus energy dissipation (below) for the kink collective (translation) coordinate. In fact the collision time decreases along $b_1(u_{sG})$ as u_{sG} increases, until approximately $b_1(max)$, and then increases again since the actual collision velocity decreases with further increase of u_{sG} (Fig. (3) of Wysin et. al. (1982)). This explains the qualitative shape of $b_1(u_{sG})$ in Fig. 4.

(2) Region II: For convenience we will drop the dependent variable u_{sG} from the arguments of critical fields. For $b_1<b<b_2$ the pair collides and forms a bound state (e.g. Fig. 5b): a "breather". As mentioned above, this region extends all the way to b=0 (as $u_{sG} \to 0$). This binding is reminiscent of bound state formation in the $S\bar{S}$ collisions for, e.g. ϕ-four (Campbell et. al. 1983) or double sine Gordon equations(Peyrard and Campbell 1983). The small fluctuation frequency spectrum in these systems includes an additional (to the zero frequency translational mode) bound state corresponding to localized internal soliton oscillations. The presence of this additional mode, which can remove energy from the translational mode during a $S\bar{S}$ collision, gives

rise to interesting effects including the breather formation at low velocities and "windows" in the initial energy (in the region between a breather formation and a hard core repulsion) where the $S\bar{S}$ pair collide, undergo one (or more) bounces and then separate. These windows have almost self-similar structures depending on the number of bounces the pair executes before finally separating to infinity. In as much as the fluctuation spectrum of an EPF soliton contains an additional bound state (Kumar 1982, Magyari and Thomas 1982), we expect windows here also and indeed find evidence for them. The breather period shown in Fig. (6) illustrates an example of this feature. The collision corresponds to u_{sG}=0.4. The behaviour for low fields is as expected, the period diverging at $b=b_1$, in anticipation of sG-like transmission for $b<b_1$. Approaching the large field region, there is a window between $0.1258 < b < 0.1289$ where the pair is transmitted. Finally for $0.14 \lesssim b < b_2(\simeq 0.16)$ the pair appears to decay into small oscillations before entering region III for $b>b_2$.

(3) Region III: For $b_2<b<b_3$, the $S\bar{S}$ pair is reflected after the collision (e.g. Fig. 5c). Basically, a soliton approaching the collision on branch I or II, after the collision is transferred to branch III moving in the opposite direction with a velocity larger than the incoming velocity. During this collision process the predominant energy transfer is from magnetic field energy to anisotropy energy, since θ_m (see section 3a) increases monotonically -- see Figs. (7a) and (8).

This region also has interesting "window" structure. For illustration we choose b=0.21 and describe the final states as a function of u_{sG}. After a collision in the middle of the chain the solitons separate. As they reach the ends, because of the periodic boundary conditions, they undergo another collision. Thus even in this case of reflection, the soliton dynamics becomes

a sequence of collisions; all the odd numbered collisions occur in the middle while the even ones occur at the boundaries.The sequence of final states for b=0.21 is then as follows: For u_{sG}=0.1, the pair is annihilated after the first bounce . For u_{sG}=0.2, after the first bounce it emerges as a pair on branch III. The next collision takes place at the chain ends and leaves the reflected pair on branch III. For u_{sG}=0.3 however, the initial collision gives rise to a branch III pair, but the next collision at the chain end leads to a branch II pair. For successive collisions, then, the final state oscillates between branch II and branch III. On both branch I and II, the soliton profile is such that $\theta_m>0$ for u>0. On branch III, however, $\theta_m>0$ for u<0. Taking these features into account together with the monotonicity of θ_m with u (Fig. 7a) the collisions in region III can be physically motivated in terms of whether $\theta_m=0$ (and $\dot{\theta}_m\neq0$) at the middle of the collision, or whether $\theta_m=\theta_m^o$ and $\dot{\theta}_m=0$ (where θ_m^o is the value for a static soliton). In the former case we would expect no branch transfer (none is observed), while in the latter case (observed at larger u_{sG}) there is branch transfer. The same reasoning explains why branch II to branch II transfer is not observed, whereas branch III to branch III is, as in Region IV:

(4) Region IV: For $b>b_3$, the incoming solitons are on branch III (e.g. Fig. 5d). They undergo reflection and emerge on the same branch. The further sequence of collisions (in the center and at the chain end in turn) repeats the process. Again this is physically sensible, since $\theta_m=0$ and $\dot{\theta}_m<0$ at the middle of the collision (c.f. Fig. 7b).

4. Conclusions and Discussion

To summarize our results: starting from a sine Gordon soliton initial condition, we have studied the dynamics of solitons in an EPF chain. The objective has been to explore the applicability of a sine Gordon type description for nonlinear dynamics. The energy dispersion appears to consist of three qualitatively different branches. Branch I corresponds to $E \propto u^2$, however the effective mass is larger than the sG value and depends sensitively on magnetic field. Branch II corresponds to a larger spin deviation from the easy plane. On this branch, the energy of the soliton increases with decreasing velocity and finally reaches the energy of a second static texture. The latter corresponds to a solution where the energy is a maximum as a function of the angle with respect to the easy plane. As a consequence of this energy maximum, the energy dispersion around this texture is an inverted parabola (negative mass). The other arm of this parabola (for $u<0$, branch III) decreases monotonically until the soliton width diminishes to a lattice spacing.

The collision of an $S\bar{S}$ pair, again initiated with a sG pair, gives rise to a variety of final states described in a phase diagram, Fig. (4). The low field collisions are sG like. With increasing field, there is a regime where $S\bar{S}$ forms a bound state, a breather. Further increase in field leads to reflection of the pair. In the breather regime there are windows corresponding to resonant energy transfer between the soliton's translational mode and the internal modes. In the reflection scattering region there are further details in the phase diagram where a branch II pair emerges as a branch III pair, reverting to a branch II pair at the next collision. Otherwise a branch II pair, after turning into a branch III pair remains on that branch during further collisions. Analytical work is in progress to

clarify these regions and the various physical factors affecting them.

For the quasi-one-dimensional easy-plane ferromagnet $CsNiF_3$, the parameter $\alpha \equiv 2A/J = 0.382$ (Steiner 1981, 1982). We have performed a limited number of runs with this value of α. If the discreteness effects are not critical, the soliton dynamics should be governed essentially by the parameter $b = \beta/\alpha$ (see section 2). The chosen values of β were 0.0342 (B=5 kG) and 0.205 (B=30 kG), these both lie in the region where $S\bar{S}$ collision gives rise to breather modes in the final state. Such a behaviour raises a fundamental issue. Namely, in the analyses of statistical properties for $CsNiF_3$ (thermodynamic and neutron scattering) solitons have been assumed to be nearly independent quasiparticles. The assumption is justified on the basis of substantial soliton integrity during collisions. If, however, the collisions predominantly give rise to generalized breathers (including the Heisenberg pulse-like solutions (below)), the fundamental excitations in $CsNiF_3$ then become these breathers and the statistical properties should be carefully reconsidered in light of results here. Such a reexamination is under consideration at the moment, and complements existing arguments (Bishop,1981a, 1981b) for the dominant influence of breathers even in the sG limit. Clearly the effect of damping on breather lifetimes needs to be considered. However, it is worth noting that the strong deviations from ideal sine Gordon $S\bar{S}$ collision which we have found are likely to have an equally serious influence on the thermal nucleation of $S\bar{S}$ pairs--i.e., thermal nucleation will predominantly generate breathers and not free solitons.

The analysis in this paper refers to a classical system. The importance of quantum effects has been discussed by several authors. However, no definite conclusions can be drawn as yet. Maki (1980) has derived a quantum renormalization of the sine Gordon soliton energy E_o, resulting in the

reduction of E_o by 20% (for B = 5kG) in agreement with a wide variety of experiments. Mikeska (1982), however, has noted that if the sG assumptions (A large) is relaxed and spin excursions off the easy plane are allowed (albeit perturbatively), the quantum renormalization of E_o is only 10%, thereby worsening the agreement with experiments.

Our analysis involves the parameters $\alpha = 2A/J$ and $\beta = g\mu_B B/JS$ (and in the continuum limit $b = \beta/\alpha$). If we interpret Maki's results on renormalization of mass $m = (\sqrt{2AB})$ and energy E_o as the dressing of coupling constants A and J, the parameter β increases due to the quantum fluctuations. The parameter α plays the role of the bare coupling constant in the quantum theory--leading to an increase in an effective b. In as much as results described here support the view that a larger b leads to larger deviations from a sine Gordon picture, one might argue that quantum effects lead the system further away from a sG description in terms of an ideal gas of solitons.

The importance of our conclusions for real materials is further emphasized by the recent observations of Kopinga et. al. (1982, 1983) on CHAB ($(C_6H_{11}NH_3)\ CuBr_3$) and its chlorine isomorph CHAC, both easy plane ferromagnetic chains. In both of these systems, the intra chain exchange constants are of order 50K but the anisotropy energy is much smaller. These are also $S = 1/2$ spin chains. As a result the nonlinear properties should be even further from a sine Gordon description than, say $CsNiF_3$. This conclusion is qualitatively corroborated by the experiments. As for $CsNiF_3$, the specific heat and spin-lattice relaxation measurements have been analyzed in terms of an effective sine Gordon theory where the soliton energy is treated as an adjustable parameter. Whereas known values of J and B would yield for the soliton energy $E_o = 10.85\sqrt{B}$ K, the experiments yield $E_o = 8.4\sqrt{B}$ K, roughly

the same reduction as in $CsNiF_3$. Because of small A (and therefore a small quantum coupling constant A/J) the quantum effects are weaker. We believe that the deviation from sG theory in these experiments really originates in the finite excursion of spins away from the easy plane and the resulting anomalous nature of nonlinear excitations. A careful analysis is in progress.

The importance of breather bound states is further emphasized by the scaling properties of Fig. (4). The phase diagram is shown in terms of $b = \beta/\alpha$, which is all that is needed except for discreteness effects. While the sG properties are clearly seen in the small b regime, $S\bar{S}$ collisions imply a closer affinity between $CsNiF_3$ and the moderate to large b region. In that case, the interesting limit to study for the Hamiltonian (Eq. (1)) becomes $\alpha = A/J \to o$ (and perturbations therefrom). In this limit, the ferromagnetic chain becomes isotropic (in exchange interaction) and exact results are known for the continuum equations, since these become exactly integrable, (Bishop 1980,1981). In particular, the principal excitations are breather-like modes which correspond to "pulses" in the angle of declination with respect to the magnetic field axis. Thus, the single soliton solution in the limit $b \to \infty$ should become the (one) exact soliton of the isotropic model (Skylanin, 1979). Analytic work is in progress to demonstrate this equivalence. An important outcome of this calculation is expected to be the profile of nonlinear excitations in the high field limit (c.f. Figs. (4) and (7.b)). Note also that <u>two</u> types of nonlinear excitations are possible for $b<b_c$ (kink-like and breather-like solitons). However, for $b>b_c$ only <u>one</u> type survives, as we see both from our single soliton and $S\bar{S}$ collision studies (consistent with the isotropic Heisenberg limit). Furthermore, the <u>topology</u> of the single soliton <u>changes</u> for $b>b_c$ from kink-like to pulse-like. ... this system: they correspond to the maximum of $E(\theta_m)$ for $b>b_c$; furthermore, they

have negative mass, lowering their energy by accelerating to higher velocities (Magyari and Thomas, 1983). We believe that the natural excitations in this limit ($b>b_c$) must be closely related to the pulse solutions mentioned above in the $\alpha \to 0$ limit. Osano (1983) has also arrived at similar conclusions.

A further comment about the resonant $S\bar{S}$ scattering is in order. The resonant energy transfer between the internal modes and the translational mode depends on the presence of the former. Thus a comparison between the present system and the complementary case of Ising symmetry breaking, (Sklyanin, 1979 and Mikeska, 1981) is now possible. In the latter, the magnetic field is replaced by an easy axis and it describes antiferromagnetic, easy plane chains. In the Ising symmetry breaking case, it is easy to show that there are no internal modes associated with the solitons and therefore the resonance scattering windows do not exist. Thus we expect that ferromagnetic chains are unique in having the nontrivial $S\bar{S}$ collisions. The Ising symmetry breaking case is also exactly integrable in the continuum limit (Sklyanin, 1979) and it appears that the existence of integrability and of bound states are mutually exclusive here as in all other known true soliton equations. A related observation is that the analagous single soliton phase diagram to Fig. (1) is in fact quite similar (Mikeska, 1981), except that $b_c \to \infty$. This is again consistent with the absence of any internal "mode softening", which occurs with magnetic field symmetry-breaking. Likewise, the exact bound state ("breather") solutions known for the Ising symmetry-breaking case (Sklyanin, 1979) form a disconnected set from the single solitons with no possibility for windows or resonances.

To conclude, then, we emphasize the unusual features of an EPF chain demonstrated by our numerical simulation. This simulation has stimulated considerable analytic work, in progress at the moment, to fully analyze the

nonlinear properties, and their experimental consequences for materials such as $CsNiF_3$ and CHAB.

References

Bishop, A. R., 1980, Z. Physik B37, 357; 1981, Z. Physik B44, 185; 1981, J. Phys. C14, 1417.

Campbell, D. K., Schönfeld, J. F. and Wingate, C.A., 1983, Physica D, to be published.

Kerr, W. C., Baeriswyl, D., Bishop, A. R., 1981, Phys. Rev. B24, 6566.

Kopinga, K., Tinus, A. M. C., and deJonge, W. J. M., 1982, Phys. Rev. B25, 4685; 1983, preprint.

Kumar, P., 1982a, Phys. Rev. B25, 483; 1982b, Physica D5, 359.

Kumar, P. and Samalam, V. K., 1982, Phys. Rev. Lett. 49, 1278.

Liebmann, R., Schöbinger, M. and Hackenbracht, D., 1983, J. Phys. C16, L633.

Magyari, E. and Thomas, H., 1982, Phys. Rev. B25, 531; 1983, J. Phys. C16, L535.

Maki, K., 1980, J. Low Temp. Phys. 41, 327.

Mikeska, H. J., 1978, J. Phys. C11, L29; 1982, Phys. Rev. B26, 5213.

Mikeska, H. J., 1981, "Physics in One Dimension", eds. J. Bernasconi and T. Schneider (Berlin: Springer-Verlag), p. 153.

Osano, K., 1983, preprint, University of Hanover.

Peyrard, M. and Campbell, D. K., 1983, Physica D to be published.

Sklyanin, E. K., 1979, Sov. Phys. Dokl. 24, 107.

Steiner, M., 1981, Physics in One Dimension, ed. J. Bernasconi and T. Schneider, (Berlin: Springer-Verlag).

Steiner, M., 1982, Proc. 22nd Scottish Universities Summer School; 1982, International Conference on Magnetism, Kyoto, Japan.

Wysin, G., Bishop, A. R., and Kumar, P., 1982, J. Phys. C15, L337.

Figure Captions

1. Soliton energy dispersion for different magnetic fields. The curves refer to $b = g\mu_B B/2AS = 0.13$, solid line (——); $b = 0.21$, dashed line (---) and $b = 0.42$, dash-dotted line (-•-•-). The curves are symmetric in u as further shown in Fig. (7). Below the critical field $b_c = 1/3$, there is a region for small u where $E \alpha u^2$. This region exists only for $b < b_c$. The soliton energy is normalized with respect to the energy of a static sine Gordon soliton. Branch I (in text) refers to the low energy low velocity dispersion. Branch III refers to the backward moving soliton with negative dispersion. Branch II connects branch I with branch III.

2. The maximum angle of excursion for spins off the easy plane, θ_m, as a function of the magnetic field. This curve refers to the second static solution in Fig. (1) that acts as the boundary between branch II and branch III. The points are results from our numerical simulation and the solid line is obtained from the Liebmann et. al. (1983) Ansatz for the spin profile, described in Eq. (10).

3. The energy of the second solution (c.f. Fig. (2)) as a function of magnetic field. Points are results from numerical simulation. Solid line is obtained from the Liebmann et. al. (1983) Ansatz, described in Eq. (10).

4. Final state phase diagram for the scattering of a soliton-antisoliton

pair. The phase space here is defined by the velocity of the input sine Gordon pair, a measure of the input energy, and the magnetic field. In region I, at low magnetic field, the pair obey sG dynamics (they pass through each other). In region II, they form a breather-like bound state (see Fig. (6)). In region III, they are reflected reminiscent of hard core collision observed in ϕ^4 or double sine Gordon equations. While a similar reflection takes place in region IV, the difference between these regions (III and IV) lies in the relationship between the signs and magnitudes of the deviations from the easy plane and the soliton velocity. (See Section 3 for details).

5. Details of collisions in various regions described in Fig. (4). a,b,c and d, respectively, refer to regions I, II, III, and IV of Fig. (4).

6. Breather period, T, in region II as a function of magnetic field b for $u_{sG} = 0.4$. The boundary between regions I and II is characterized by a divergence in T. However, no such divergence takes place at the boundary between II and III. Instead, preceding this boundary there is a window characteristic of resonance scattering (Sec. 3).

7. A symmetrized dispersion curve for (a) $b < b_c$ and (b) $b > b_c$. This figure is presented to motivate the physical differences underlying collisions in region III and IV. In region III, corresponding to (a), the $S\bar{S}$ pair after collision emerges with increased velocity lying on the outer branch of the dispersion curve, corresponding to a reversed relationship between the sign of θ_m (off easy plane angle) and the propagation velocity (see Sec. 3). The arrows indicate the direction of

increasing θ_m.

8. Various components of the energy density during collision: E_A, E_B and E_C refer to anisotropy, magnetic field and exchange components, respectively (see Eq. (1)). The figure corresponds to $u_{sG} = 0.6$ and $b = 0.13$ in region III. Also shown as functions of time are the (numerically determined) instantaneous soliton velocity, u, (in units of c, the spin wave velocity) and the maximum off easy-plane angle (i.e., at the soliton center), Δ, expressed in units of this quantity for the initial sine Gordon soliton (0.532 radians).

FIG. 1

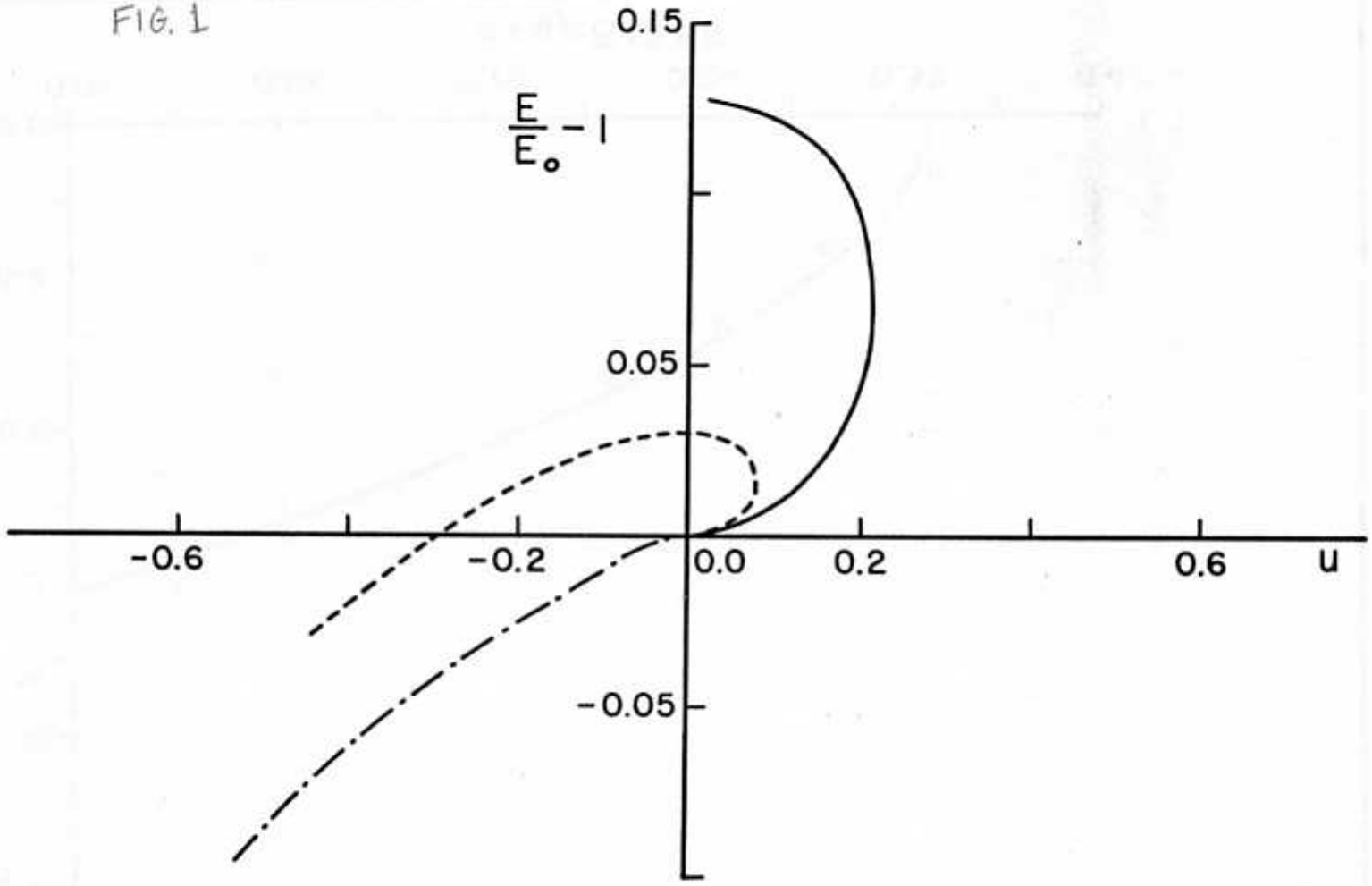

FIG. 2

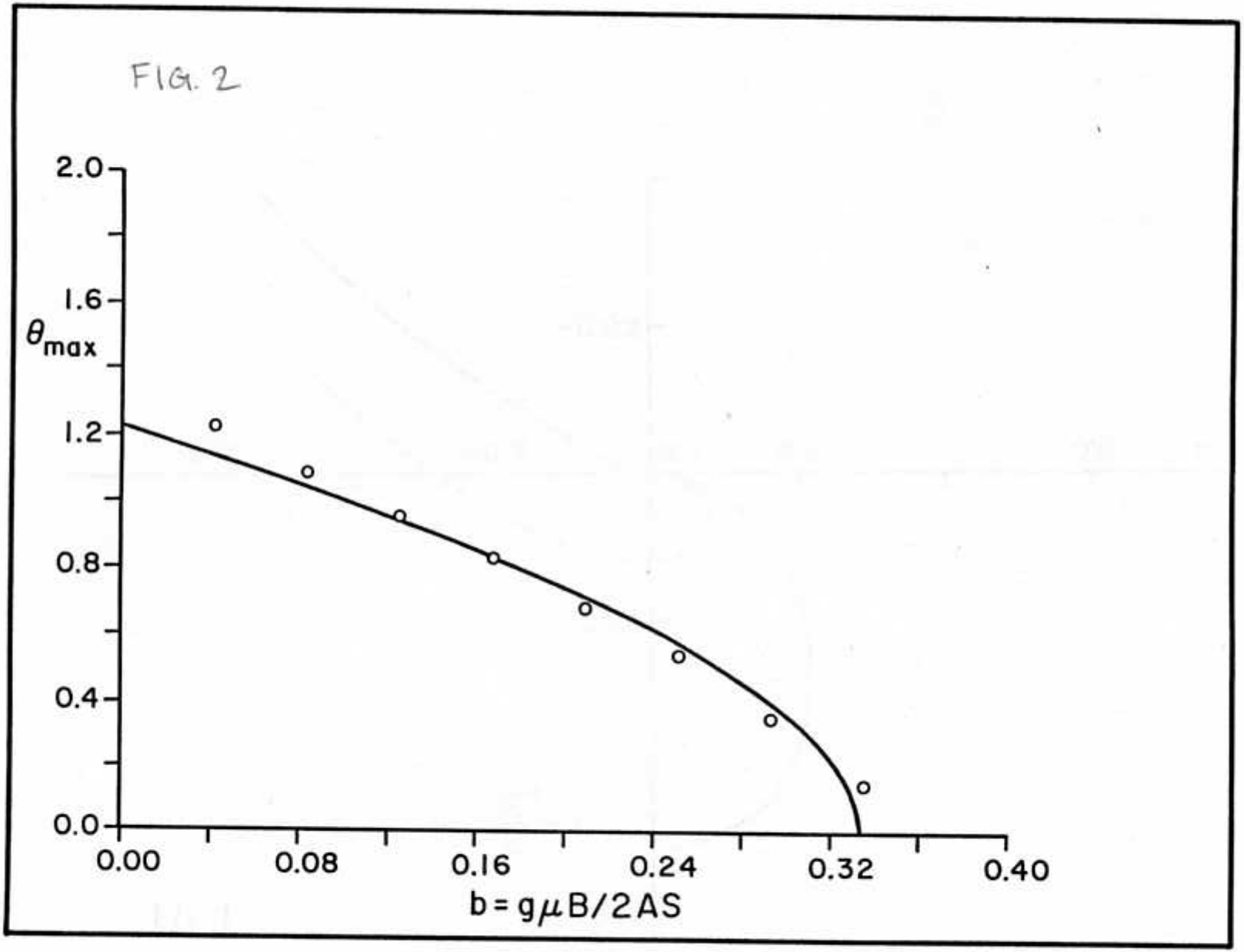

FIG. 3

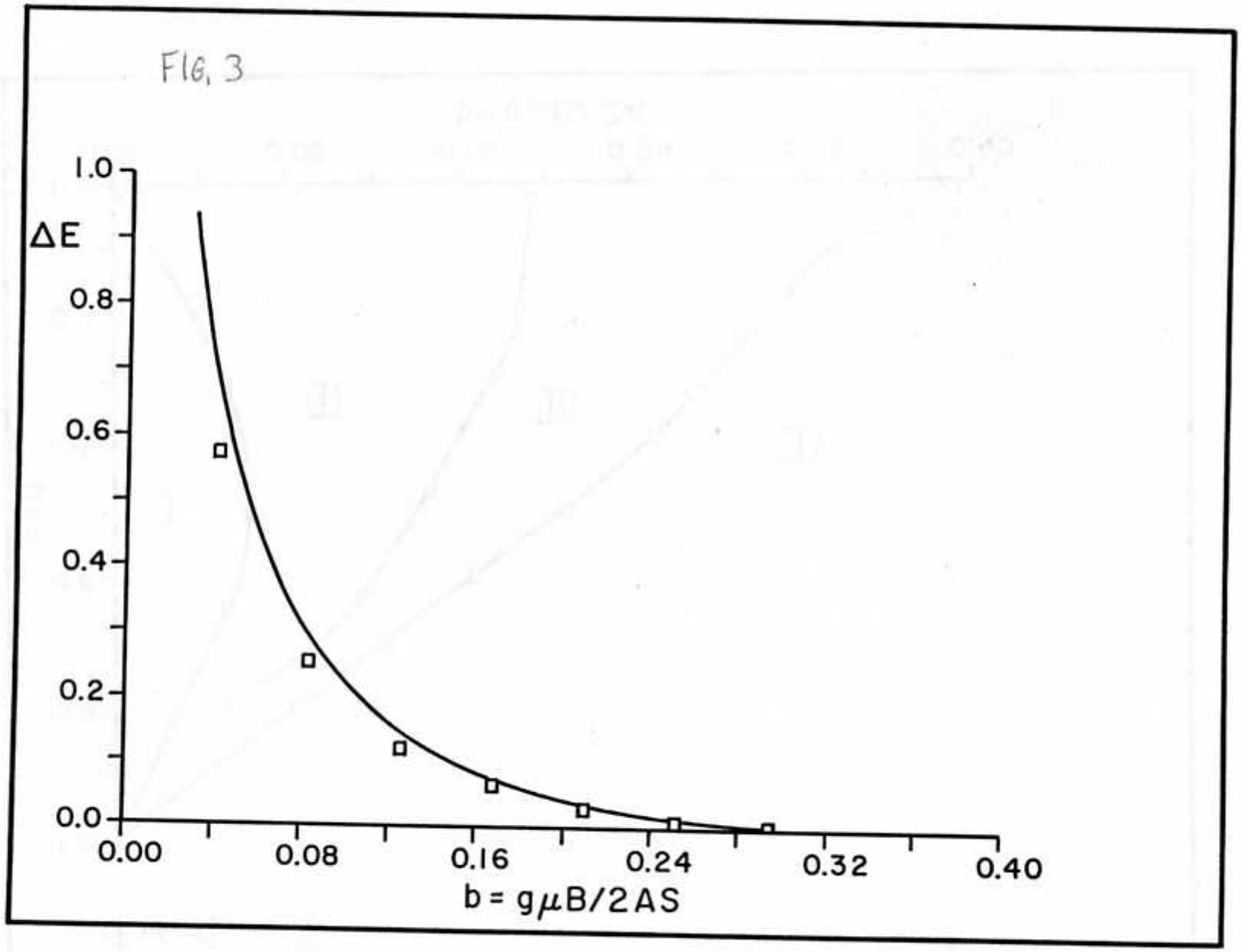

FIG. 4

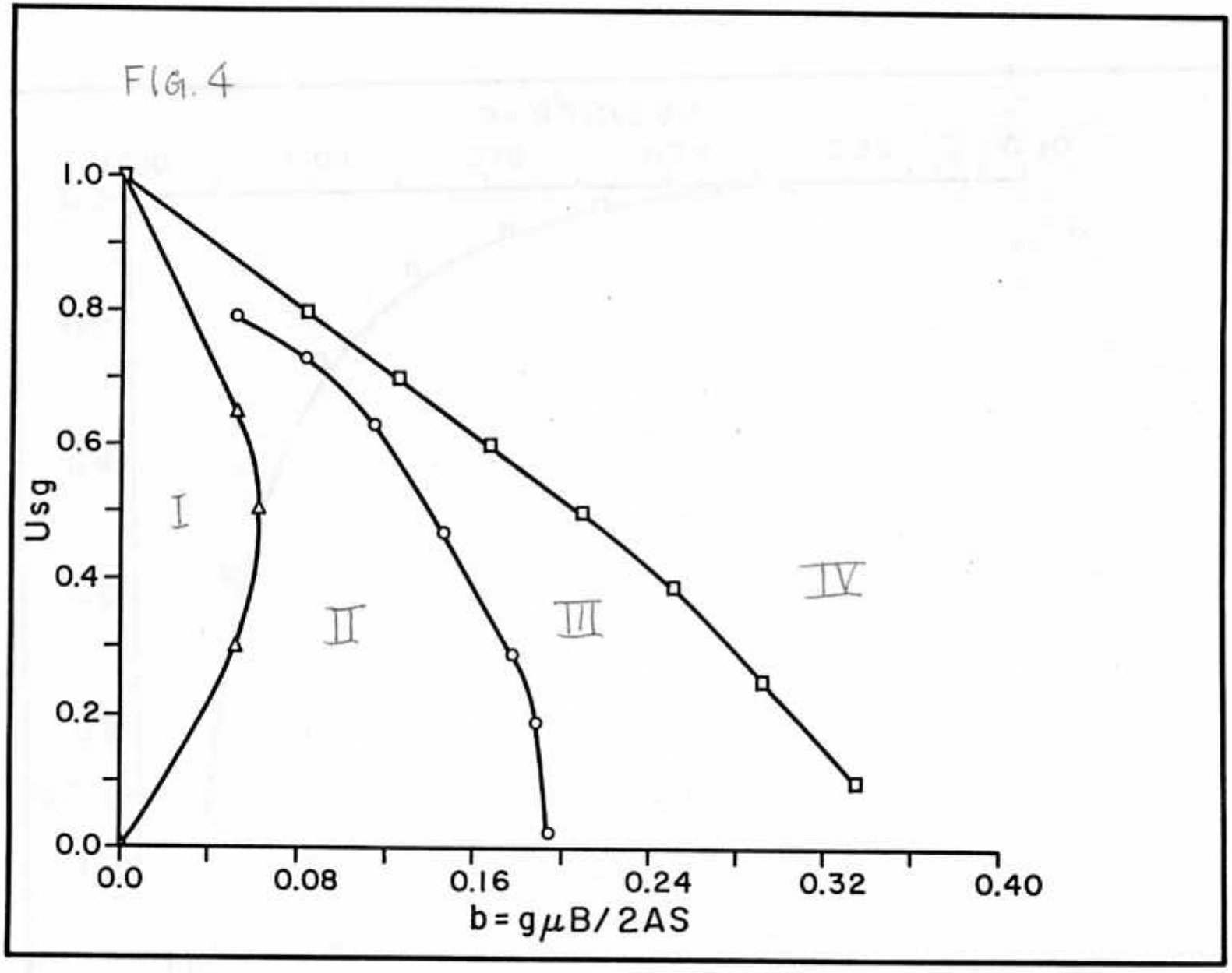

FIG 5. t_1

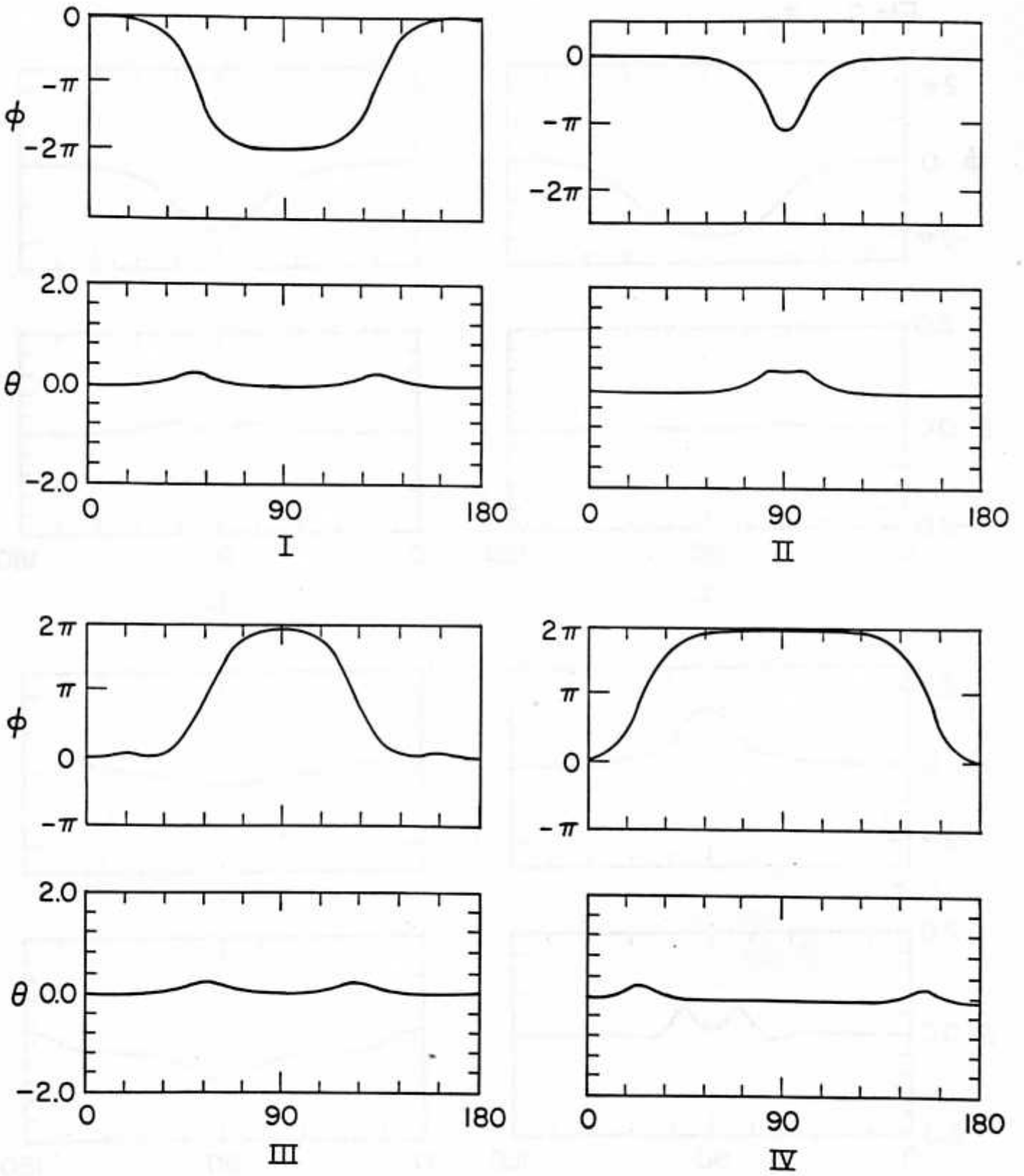

FIG 5. t_2

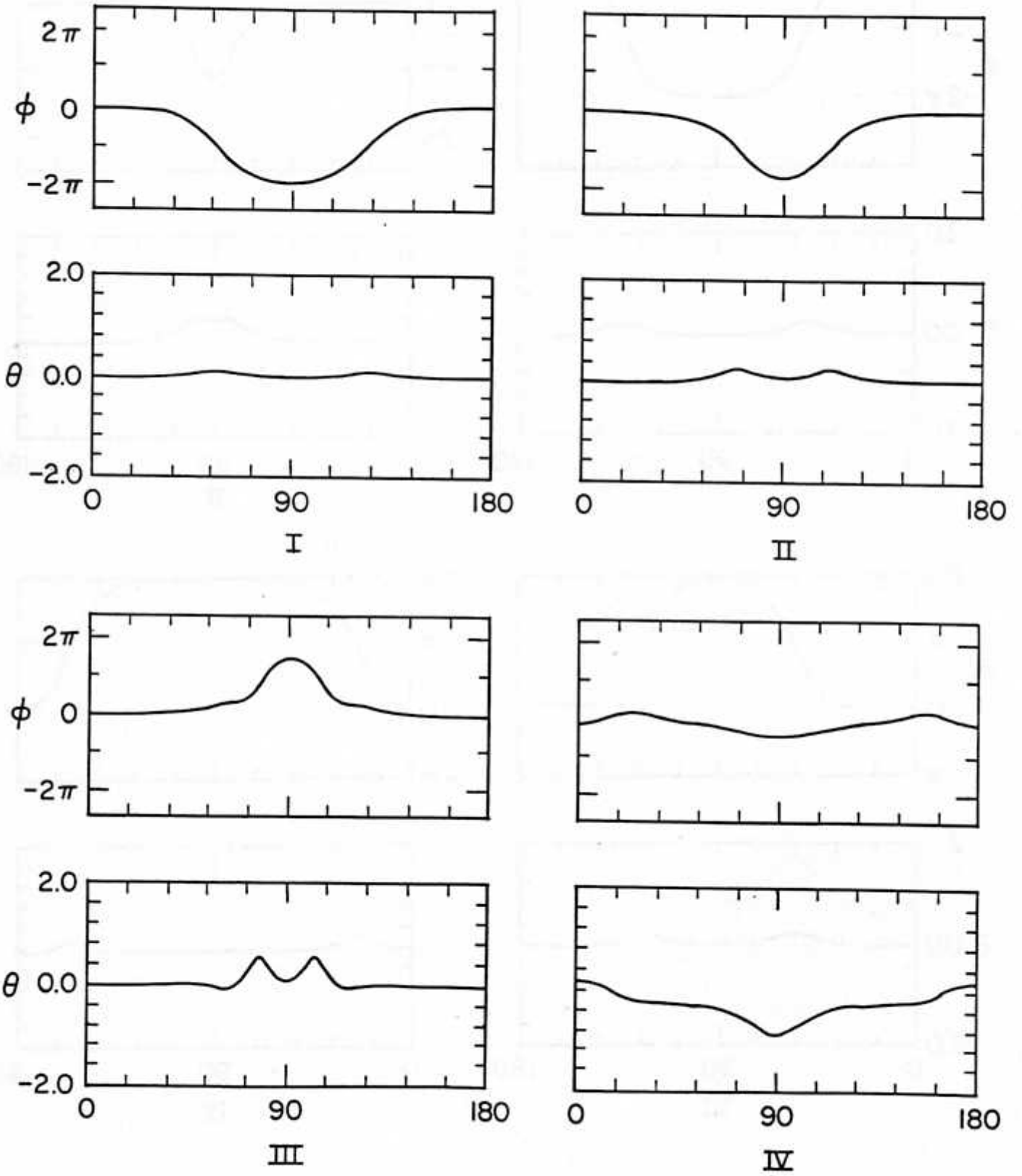

FIG 5. t_3

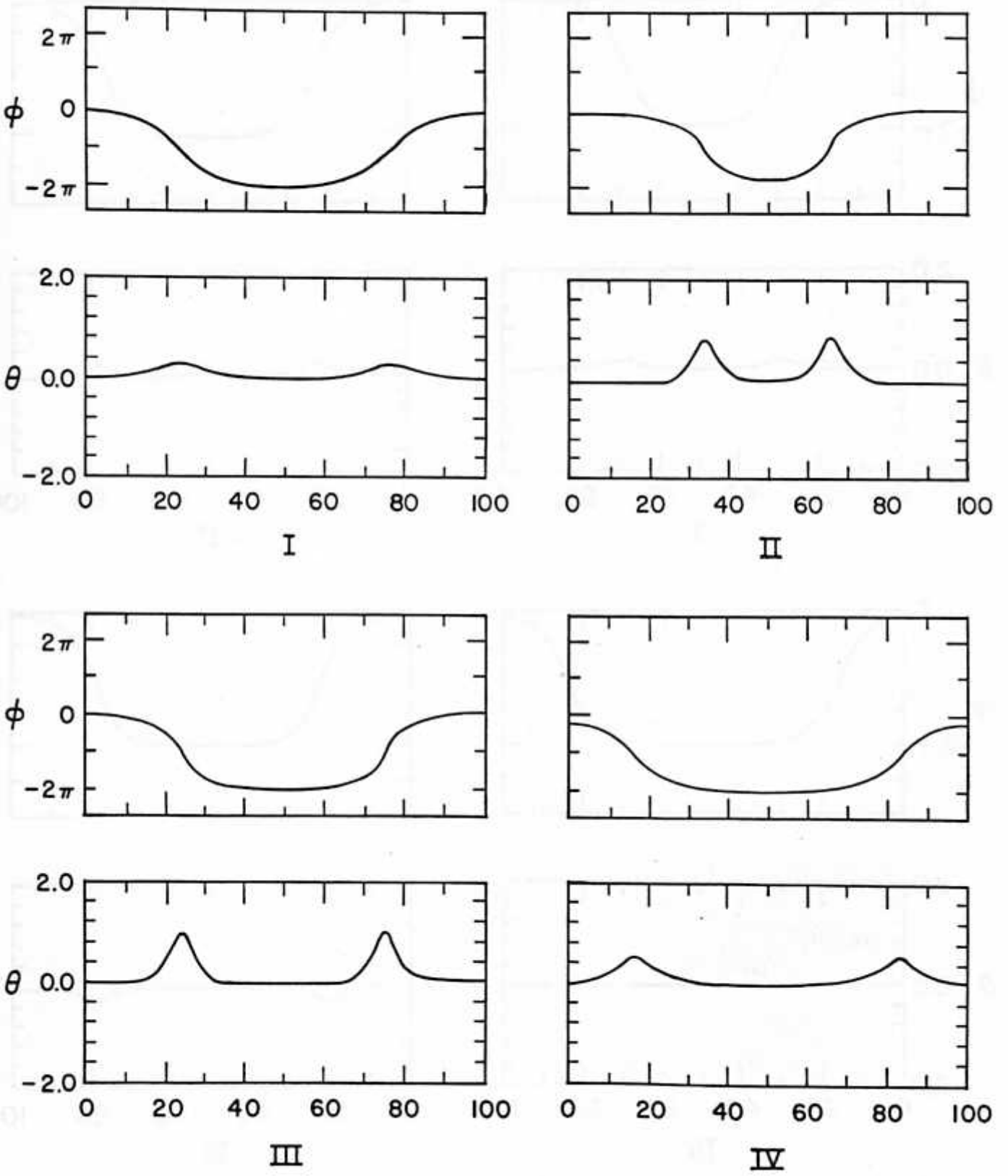

FIG 5. t_4

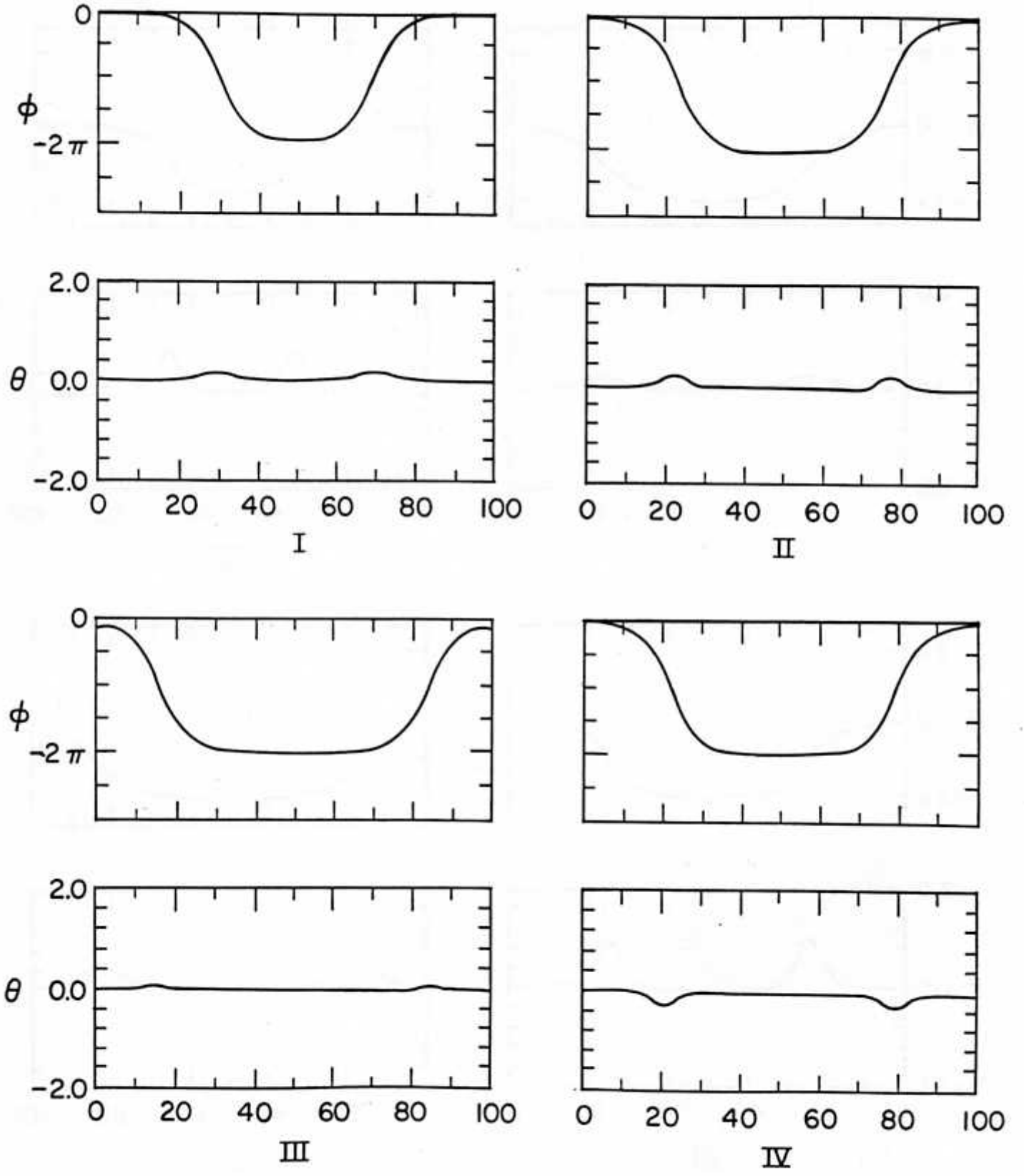

FIG. 6

FIG 7 a).

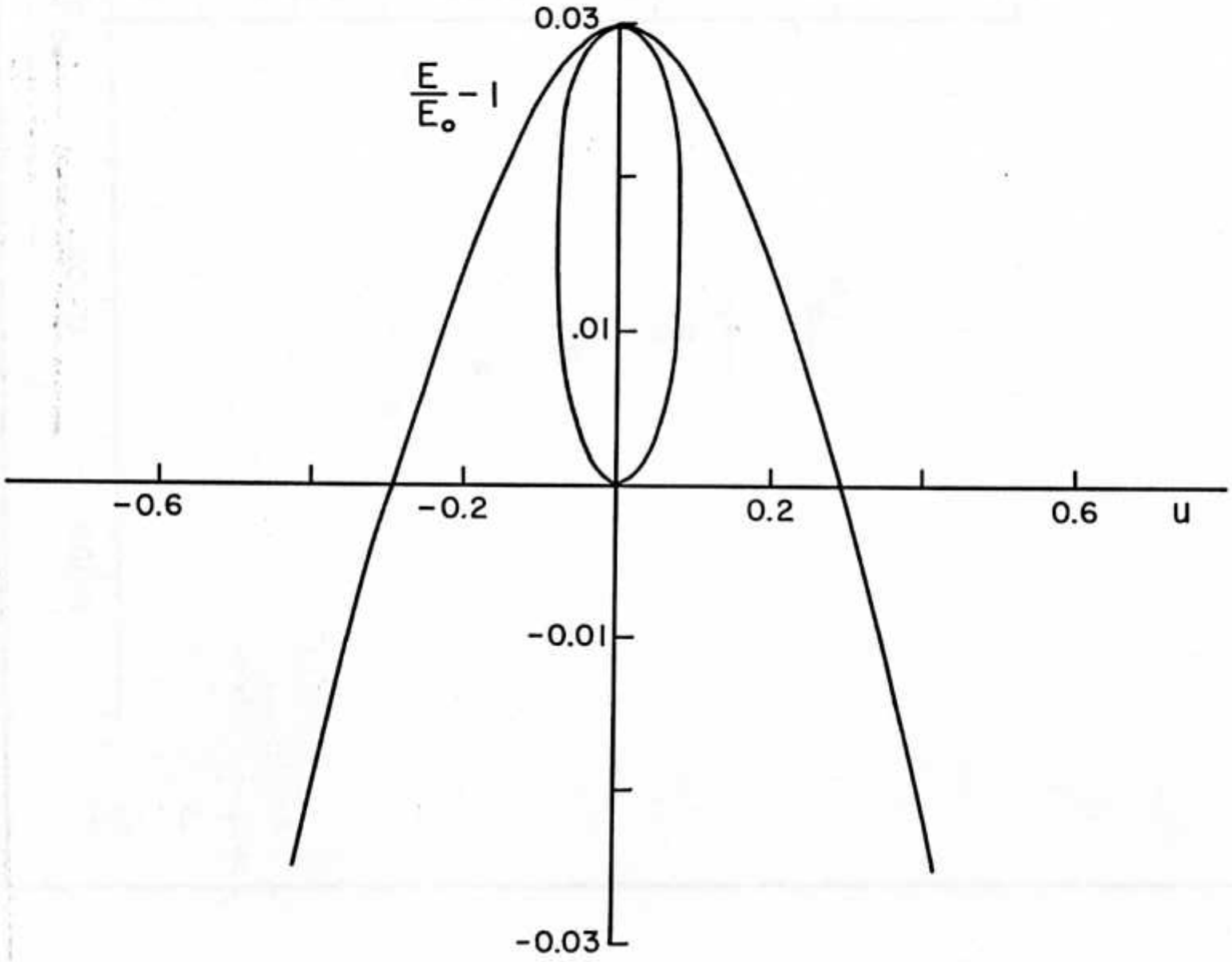

FIG 7 b)

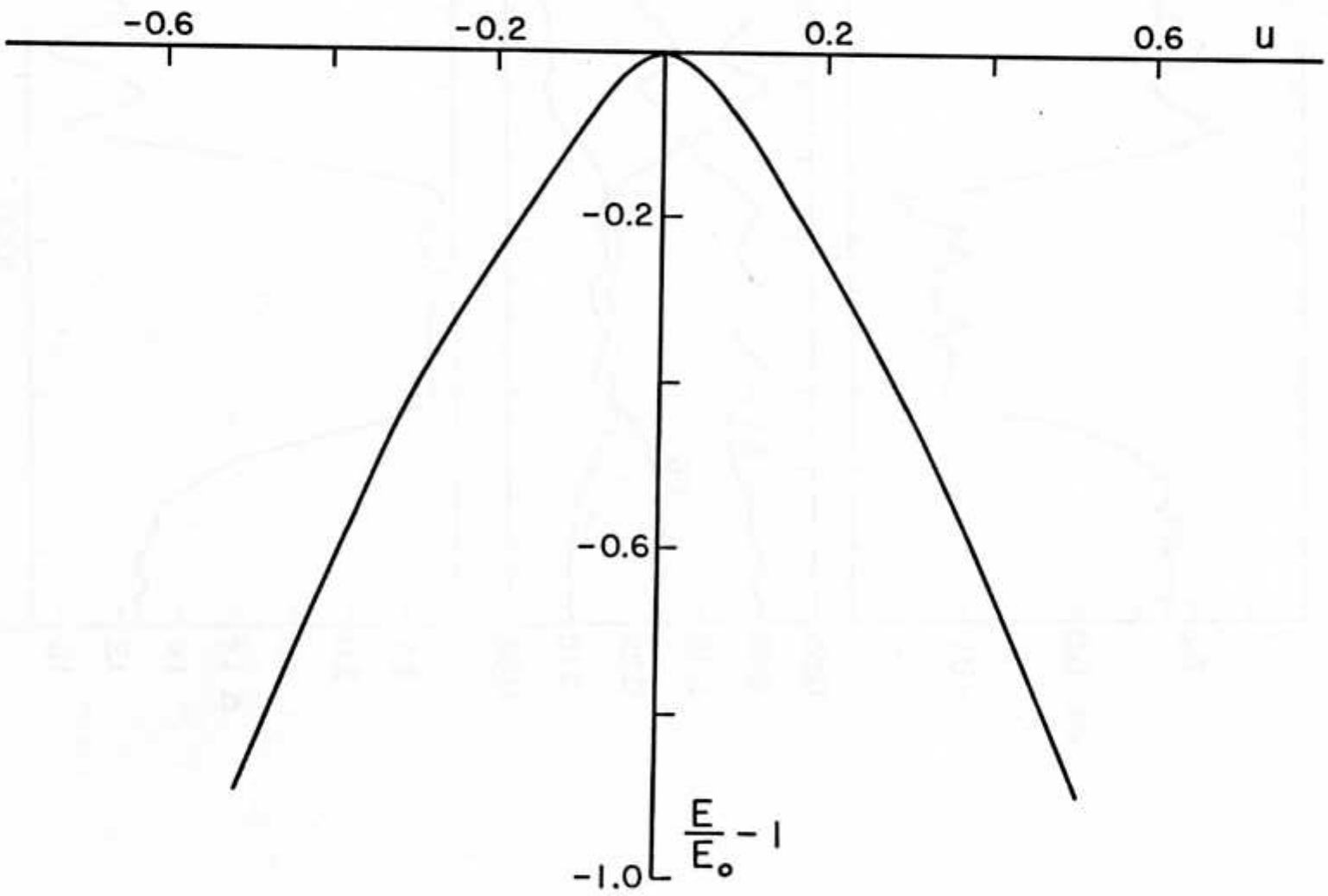

FIG. 8.

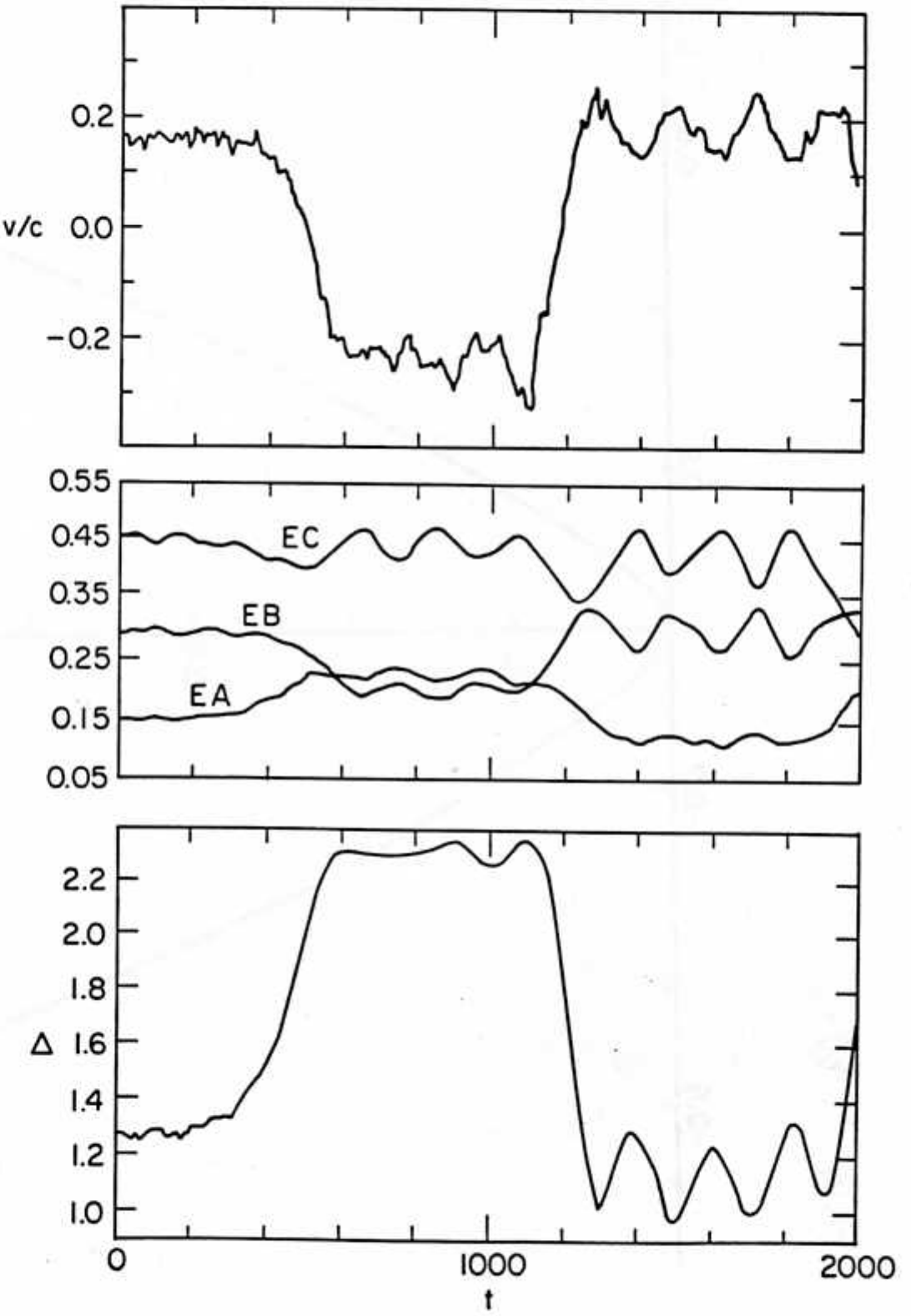
v/c
0.2
0.0
-0.2
0.55
0.45
0.35
0.25
0.15
0.05
EC
EB
EA
Δ
2.2
2.0
1.8
1.6
1.4
1.2
1.0
0
1000
2000
t